J Mater Sci: Mater Electron
DOI 10.1007/s10854-017-7637-4

Studies on chemically synthesized PbS thin films for IR detector application

Ashwini B. Rohom[1] · Priyanka U. Londhe[1] · Priya R. Jadhav[1] · Ganesh R. Bhand[1] · Nandu B. Chaure[1]

Received: 20 June 2017 / Accepted: 1 August 2017
© Springer Science+Business Media, LLC 2017

Abstract Lead sulfide (PbS) is an important binary semiconductor material due to its narrow direct band gap energy (0.41 eV, for bulk) and a large exciton Bohr radius (18 nm). In the present work, PbS thin films were deposited by using chemical bath deposition method and characterized thoroughly with the help of range of characterization techniques to study various properties. X-ray diffraction confirms the formation of cubic structure of PbS. Upon thermal heat treatment the crystallinity of the sample was found to be increased remarkably. The optical band gap 1.23 and 1.10 eV was estimated for as-prepared and heat-treated PbS thin films. Compact, void free, densely packed well adherent growth of PbS layer was confirmed by SEM images. Triangular shaped morphology was observed for as-deposited samples, whereas agglomerated cauliflower shaped clusters were formed upon annealing. Pb-rich layers were confirmed from energy dispersive X-ray analysis upon annealing due to the evaporation of elemental sulfur present at grain boundaries and on the surface of sample. Both samples revealed Schottky behavior under dark and infra-red (IR) illumination condition. The increased photocurrent measured under IR illumination demonstrated that PbS was a good candidate for IR detector. The decreased ideality factor calculated for annealed sample revealed the enhancement in the crystallinity and less leakage current through grain boundaries.

✉ Nandu B. Chaure
n.chaure@physics.unipune.ac.in

[1] Department of Physics, Savitribai Phule Pune University, Pune 411007, India

1 Introduction

Semiconductors are an important class of materials due to their ability to tune electrical, optical and opto-electronic properties and also for their applications in micro and optoelectronics, nonlinear optics, photocatalysis and energy conversion industries [1–3]. Lead sulfide (PbS) is an important IV–VI semiconductor material because of its direct band gap, ~0.41 eV and exciton Bohr radius of ~18 nm at room temperature [4, 5]. PbS has been used in photodetectors, solar cells, infra-red (IR) detector, biosensors, deep tissue imaging, etc [6–8]. PbS can be used to measure radiation in either of two ways, by measuring the photocurrent, or by measuring the change in the material's electrical resistance when photon hits. Measuring the resistance change is the more commonly used method [9, 10]. At room temperature, PbS is sensitive to radiation at wavelengths between approximately 1 and 2.5 μm. This range corresponds to the shorter wavelengths in the IR portion of the spectrum. Only very hot objects emit radiation in these wavelengths. The combination of such properties makes PbS suitable for efficient electroluminescent devices, such as tunable near-IR detectors, solid state lasers and biological sensing applications [11–13]. Various deposition techniques, such as electrodeposition [14], pulsed laser deposition [15], spray pyrolysis [16] and chemical bath deposition (CBD) [17] have been used to deposit PbS layers. Several attempts have been made to synthesize the PbS nanoparticles for various applications [18, 19]. CBD is one of the cheapest methods to deposit thin films and nanomaterials, as it does not require expensive equipments, scalable and can be employed for large area deposition. CBD has been successfully utilized to grow various semiconductor thin films including, PbSe [20], CdS [21], CdSe [22], ZnO [23], ZnS [24]. Long time ago, in 1933 Brückmann had deposited PbS thin film by CBD method [25]. In the present work we have reported the growth of PbS thin films by

Published online: 08 August 2017

simple CBD onto the glass substrates using lead acetate, triethanolamine and thiourea. Especially, the electrical properties under IR illumination are investigated for both as-deposited and annealed PbS thin films.

2 Experimental details

2.1 Materials

All chemicals, lead acetate $(CH_3COO)_2Pb{\cdot}3H_2O$, triethanolamine (TEA) $(C_6H_{15}NO_3)$, sodium hydroxide (NaOH) and thiourea (CH_4N_2S) of purity at least 99% were purchased from Sigma Aldrich and used without further purification. Double distilled water (DDW) was used as a solvent.

2.2 Experimental procedure

PbS thin films were prepared by CBD technique with 0.01 M lead acetate and 0.1 M thiourea in DDW. Initially, the solution of lead acetate was vigorously stirred for half an hour. Subsequently, the TEA (complexing agent) was added drop wise into the solution. pH of the solution was adjusted to ~11 by using NaOH at room temperature. Ultrasonically cleaned microscopic plates were used as substrates. Finally, 0.1 M thiourea was added to form the PbS. The films were deposited for an hour at 80 °C with continuous moderate agitation. The prepared samples were ultrasonically cleaned in warm DDW to remove the unreached part or loosely bound particles. The samples were annealed in an air ambient at 400 °C for 30 min.

2.3 Reaction mechanism

Chemical bath deposition of any material depends on the ionic product and the solubility product. The deposition takes place when the ionic product exceeds the solubility product [26]. The PbS thin films are expected to deposit by the following reaction mechanism:

In alkaline solution the hydrolysis of lead acetate leads to the formation of $Pb(OH)_2$

$$Pb\left(CH_3COO\right)_2 + 2NaOH \rightarrow Pb(OH)_2 + 2CH_3COONa \quad (1)$$

$$Pb(OH)_2 \rightarrow Pb^{2+} + 2OH^- \quad (2)$$

Thiourea decomposes in alkaline solution and produces HS^- ions,

$$CS\left(H_2N\right)_2 + OH^- \rightarrow CH_2N_2 + H_2O + HS^- \quad (3)$$

$$HS^- + OH^- \rightarrow H_2O + S^{2-} \quad (4)$$

$$Pb^{2+} + S^{2-} \rightarrow PbS \quad (5)$$

2.4 Characterizations

The as-deposited and annealed PbS thin films were characterized with a range of characterization techniques. The structural properties were studied by means of X-ray diffraction (XRD) technique, model Bruker D8 advance diffractometer with Cu Kα anode of wavelength 0.154 nm. Optical absorption measurements were carried out by JASCO V-670 UV–Vis–NIR spectrometer. Surface morphology was studied with the help of HITACHI, S 4800 field emission scanning electron microscope (FESEM). The elemental atomic percentage concentration was obtained by energy dispersive X-ray analysis (EDAX) technique equipped with the above FESEM unit. The Potentiostat, SP 300 Biologic equipped with two probe measurement setup was employed to study the electrical properties. IR light of input power intensity 10 mW/cm^2 was used to study the electrical properties.

3 Results and discussion

The deposited PbS thin films were grayish in appearance, without powdery deposition and well adherent to the substrate. The samples were characterized thoroughly to study their various properties.

3.1 Structural properties

Figure 1 shows the XRD patterns of as-deposited and annealed PbS thin films. The diffraction peaks observed about 26.78°, 30.12°, 43.13°, 51.10° and 53.21° corresponds to (111), (200), (220), (311) and (222) reflections of cubic structure of PbS (JCPDS data file No. 05-0592). The peaks correspond to metallic Pb or its oxide was not observed. The summary of the XRD results are given in Table 1. The full width at half maximum (FWHM) has been found to decrease upon annealing the sample, which might be associated to the enhancement in the crystallinity due to the re-crystallization of layer.

The average crystallite size was calculated by using the well known classical Debye Scherrer's formula [27]:

$$t = \frac{0.9\lambda}{\beta \cos\theta} \quad (6)$$

where t is the average crystallite size, λ is the wavelength of incident X-ray, β is the value of FWHM and θ is the angle of diffraction.

The average crystallite size was estimated around ~30 and ~45 nm for as-deposited and annealed PbS thin films, respectively. These values were average of crystallite size obtained for each XRD peak. The Williamson–Hall (W–H) equation was further used to calculate values of strain and to confirm the crystallite size of the PbS samples. The FWHM can be

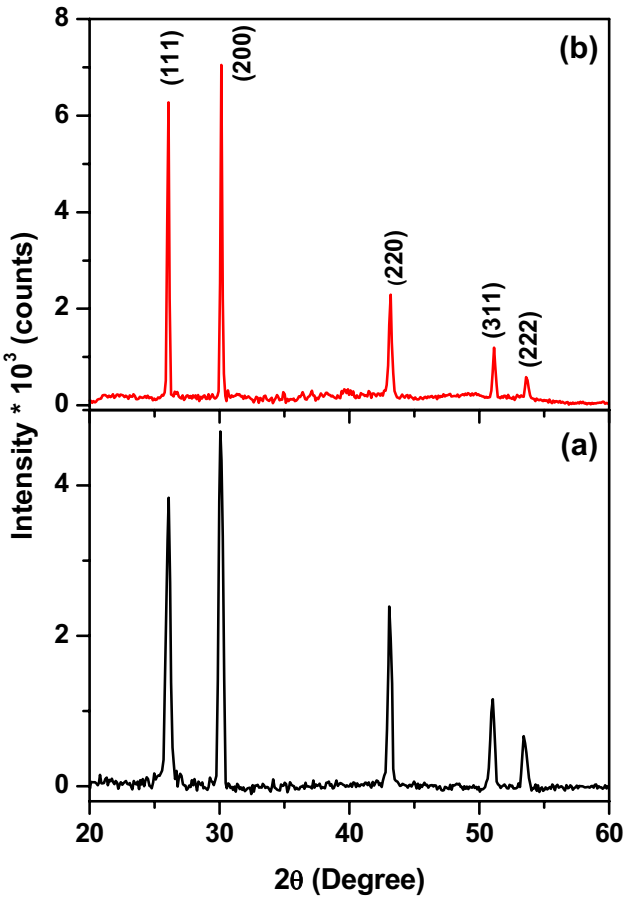

Fig. 1 XRD pattern of (*a*) as-deposited and (*b*) annealed lead sulphide thin films deposited by chemical bath deposition method

expressed as a linear combination of the contributions from strain and crystallite size through the following equation [27]:

$$\beta \cos\theta = \eta \sin\theta + \frac{\lambda}{t} \tag{7}$$

where 'η' is the strain and 't' is the average crystallite size. Slope of plot of $\beta\cos\theta$ versus $\sin\theta$ gives the values of strain, whereas the inverse of the intercept gives the value of average crystallite size. Figure 2 depicts the plot of $\beta\cos\theta$ versus $\sin\theta$ of as-prepared and annealed layers. The values of the strain, 2.05×10^{-3} and 5.46×10^{-3} were calculated for as-prepared and annealed layers, respectively. The positive value of strain indicates the presence of tensile strain in the crystal lattice [28]. The enhancement in the strain upon annealing could be due to the enhancement in the crystallite size and re-crystallization of material. The average crystallite sizes obtained by W–H equation were in good agreement with the values calculated with Debye Scherrer's equation.

3.2 Optical properties

Optical measurements performed onto as-prepared and annealed PbS thin films are shown in Fig. 3. A clear red-shift in the fundamental absorption edge of annealed sample was observed, which might be due to the increasing of particle size as well as re-crystallization of material. The absorption observed for higher wavelength to annealed sample could be associated to the drastic variation in the particle size.

The following Tauc equation was used to optimize the values of energy band gap (E_g) [29]:

$$\alpha h\nu = K(h\nu - E_g)^{\frac{n}{2}} \tag{8}$$

where K is a Richardson's constant, E_g is the band gap of the material, and n is a constant taken to be 1 for PbS as a direct band gap semiconductors. The Tauc plot $(\alpha h\nu)^2$ verses $h\nu$ shown in Fig. 4 was used to estimate the band gap values. The values of the energy band gap, 1.23 and 1.10 eV for as-prepared and annealed, respectively were estimated from the intercept of the straight-line portion of the $(\alpha h\nu)^2$ against $(h\nu)$ plot. The decreased band gap for annealed PbS layer as compared to as-deposited sample might be due to

Table 1 A summary of the XRD results obtained for as-deposited and annealed PbS thin films

PbS samples	2θ (deg)		'd' value (Å)		FWHM (deg)	Miller indices (hkl)	Phase assignment
	Standard	Observed	Standard	Observed			
As-deposited	25.96	26.00	3.429	3.424	0.331	(111)	Cubic
	30.07	30.06	2.969	2.970	0.313	(200)	Cubic
	43.05	43.08	2.099	2.098	0.292	(220)	Cubic
	50.97	51.16	1.790	1.784	0.213	(311)	Cubic
	53.41	53.66	1.714	1.706	0.255	(222)	Cubic
Annealed	25.96	26.05	3.429	3.418	0.153	(111)	Cubic
	30.07	30.12	2.969	2.964	0.133	(200)	Cubic
	43.07	43.14	2.099	2.095	0.233	(220)	Cubic
	50.97	51.06	1.790	1.787	0.201	(311)	Cubic
	53.41	53.49	1.714	1.711	0.255	(222)	Cubic

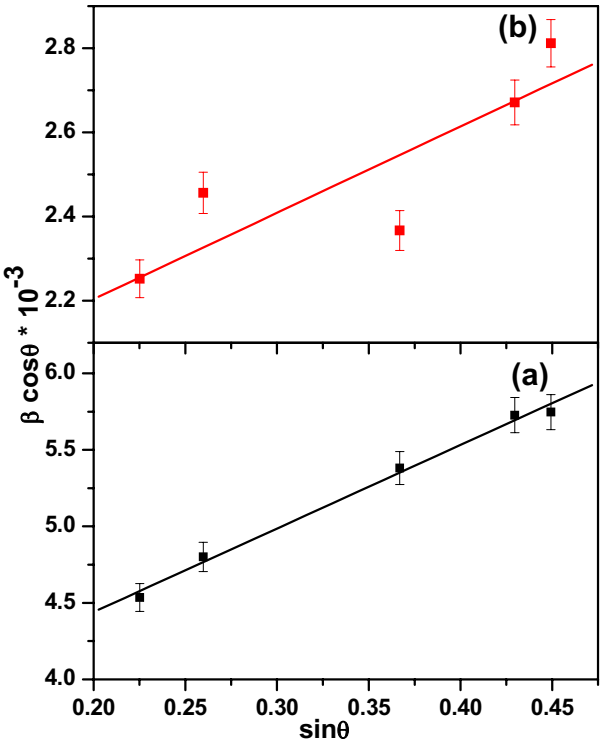

Fig. 2 Plot $\beta\cos\theta$ versus $\sin\theta$ of (*a*) as-deposited and (*b*) annealed lead sulphide thin films

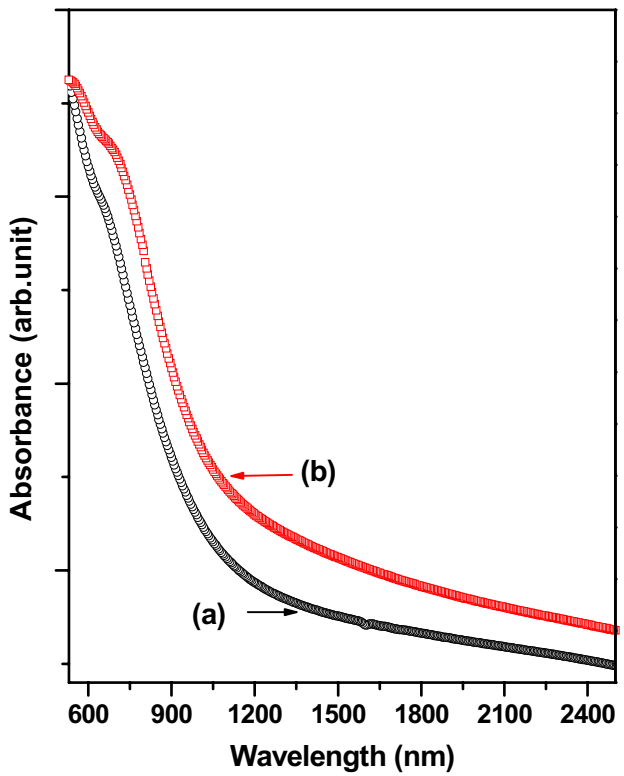

Fig. 3 Optical absorption spectra of (*a*) as-deposited and (*b*) annealed lead sulphide thin films

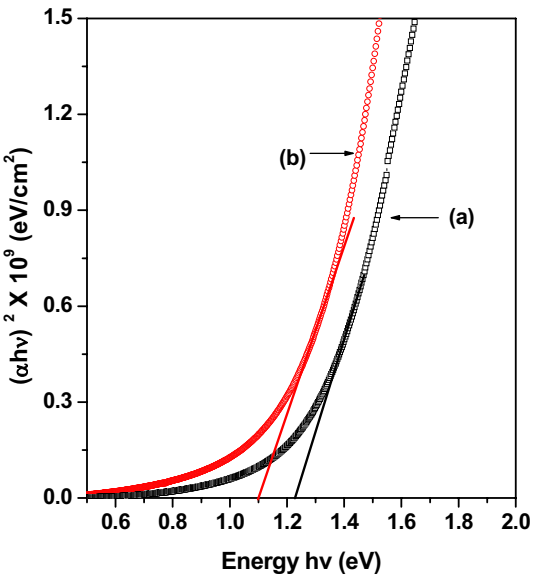

Fig. 4 Tauc plot of (*a*) as-deposited and (*b*) annealed lead sulphide thin films deposited by chemical bath deposition method

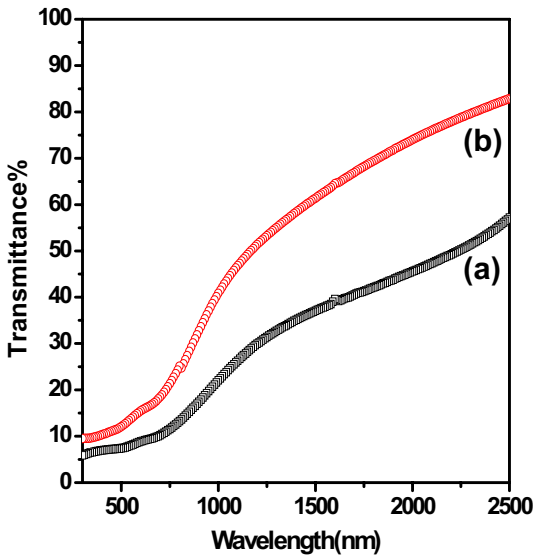

Fig. 5 Transmission spectra of as-deposited and annealed lead sulphide thin films

be associated to the increase in particle size. Figure 5 shows the transmission spectra of as-deposited and annealed PbS thin films. From transmission spectra it is observed that the as-deposited film is more transparent than that of the annealed layer. Less transmittance measured for both the layer in IR region demonstrate the suitability for IR detector applications.

3.3 Morphological properties

Figure 6 show the SEM images of as-deposited and annealed PbS thin films. A void free, compact densely packed surface morphology was imaged for both samples. Arbitrary particle growth was observed in as-deposited sample; whereas the agglomeration of small particle grows cauliflower like globular morphology can be clearly seen for the annealed sample.

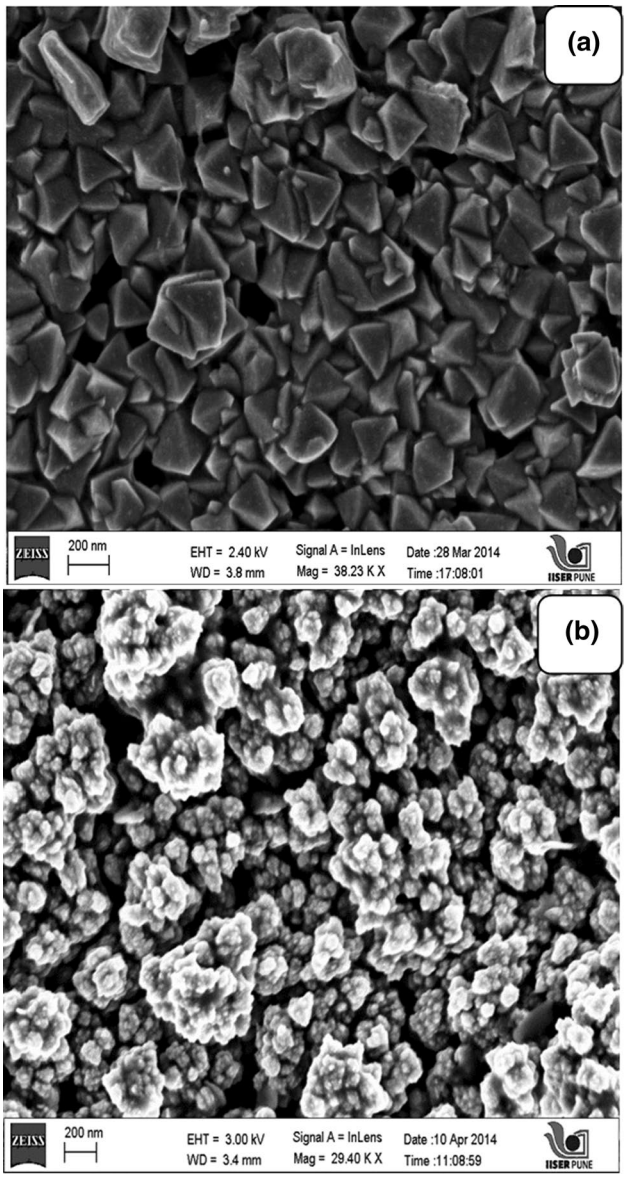

Fig. 6 FESEM images of **a** as-deposited and **b** annealed lead sulphide thin films, a and b are their corresponding magnified images

3.4 Compositional analysis

The elemental compositional analysis of PbS samples were determined using EDAX analysis. The atomic percentage concentrations obtained by EDAX analysis for as-deposited and annealed samples are summarized in Table 2. Upon annealing the contents of sulfur were found to be decreased, which might be due to the evaporation of free sulfur available at grain boundaries and top surface of the sample. These results support the electrical measurements which will be discussed in the following section.

3.5 Electrical properties

Fig. 7a, b shows the current density versus voltage (J–V) measurements carried out under dark and IR illumination for as-deposited and annealed PbS thin films, respectively. Both sample exhibits Schottky behavior under dark and IR illumination. For both as-deposited and annealed samples, nearly four times enhancements in the current density were observed upon IR illumination at ~0.5 V bias voltage as a counter part of dark condition measurements. This result is further demonstrates that the PbS layer can be used as a IR detector.

The semi-logarithmic graphs of ln(I) versus applied bias shown in inset of Fig. 7a, b were used to calculate the ideality factor. Au metal contacts of diameters of 5 mm were made on to PbS layer by thermal evaporation technique. The value of the ideality factor (A) was calculated from the slope of straight line region of the forward bias using the following relation [30]:

$$E = \frac{q}{kT}\frac{dV}{d(\ln I)} \tag{9}$$

where 'q' is the charge of electron, 'V' is the applied voltage, 'A' is the ideality factor, 'k' is the Boltzmann constant, 'T' is the temperature and 'I' is the diode current. The values of ideality factor 1.62, 1.33 and 1.54, 1.21 were calculated for dark and IR illumination condition for as-deposited and annealed samples, respectively. The decreased values of ideality factor (closer to unity) are associated to the enhanced crystallinity due to re-crystallization of material which can further reduce the leakage current in the diode.

Table 2 The elemental atomic percentage concentration obtained by EDAX for as-deposited and annealed PbS samples

PbS samples	Atomic percentage concentration (%)	
	Pb	S
As-deposited	46.97	53.03
Annealed	54.05	45.95

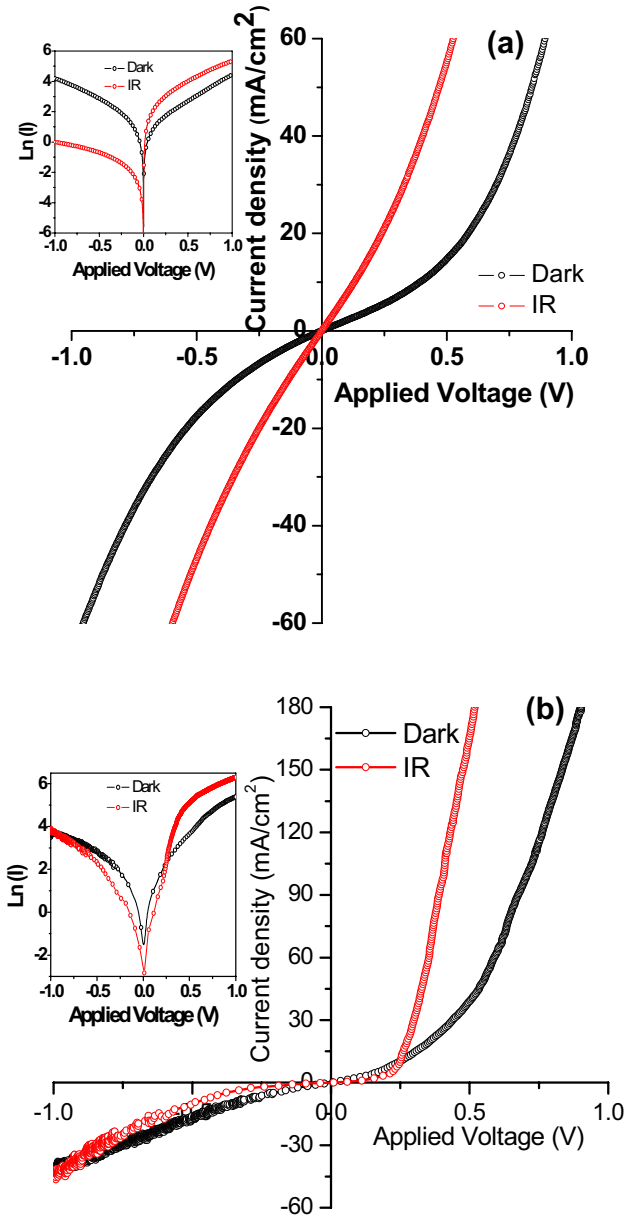

Fig. 7 Current density–voltage (J–V) curves of **a** as-deposited and **b** annealed PbS thin films measured under dark and IR illumination

4 Conclusion

A simple chemical bath deposition technique was employed to deposit PbS thin film. Highly crystalline layers with cubic crystal structure were confirmed from XRD analysis. The energy band gap values 1.23 and 1.10 eV were estimated from absorption spectra. Arbitrary shaped particles were observed in as-deposited sample, which are agglomerated and grown to a cauliflower like globular clusters upon annealing. Both samples were well adherent to the substrate without pin holes and densely packed. Pb-rich layers were confirmed from EDAX analysis upon annealing due to the evaporation of elemental sulfur present at grain boundaries and on the surface of sample. Both samples revealed Schottky behavior under dark and IR illumination conditions. The increased photocurrent measured under IR illumination demonstrates that PbS could be a good IR detector candidate. The decreased ideality factor calculated for annealed sample revealed the enhancement in the crystallinity and less leakage current through grain boundaries.

Acknowledgements The financial support from DST (SERI) Grant Ref No DST/TM/SERI/FR/124(G) in gratefully acknowledged. One of the authors ABR acknowledges the CSIR for Senior Research fellowship.

References

1. P.U. Londhe, A.B. Rohom, N.B. Chaure, RSC Adv. **5**, 89635–89643 (2015)
2. C. Rajashree, A.R. Balu, V.S. Nagarethinam, J. Mater. Sci. Mater. Electron. **27**, 5070–5078 (2016)
3. P. Cabrera, A. Arizmendi-Morquecho, J. Non-Oxide Glasses **8**, 59–66 (2016)
4. E. Yücel, Y. Yücel, B. Beleli, J. Alloys Compd. **642**, 63–69 (2015)
5. J.L. Machol, F.W. Wise, R.C. Patel, D.B. Tanner, Phys. Rev. B **48**, 2819–2822 (1993)
6. A. Slonopas, N. Alijabbari, C. Saltonstall, T. Globus, P. Norris, Electrochim. Acta **151**, 140–149 (2015)
7. S. Kaci, A. Keffous, S. Hakoum, A. Mansri, Vacuum **116**, 27–30 (2015)
8. J. Seo, M.J. Cho, D. Lee, A.N. Cartwright, P.N. Prasad, Adv. Mater. **23**, 3984–3988 (2011)
9. T. Safrani, T.A. Kumar, M. Klebanov, N. Arad-Vosk, R. Beach, A. Sa'ar, I. Abdulhalim, G. Sarusi, Y. Golan, J. Mater. Chem. C **2**, 9132–9140 (2014)
10. S. Kaci, A. Keffous, S. Hakoum, M. Trari, O. Mansri, H. Menari, Appl. Surf. Sci. **305**, 740–746 (2014)
11. S. Kaci, A. Keffous, S. Hakoum, Appl. Surf. Sci. **305**, 740–746 (2014)
12. N. Choudhury, B.K. Sarma, Thin Solid Films **519**, 2132–2134 (2011)
13. L. Truong, I.S. Moody, D.P. Stankus, J.A. Nason, M.C. Lonergan, R.L. Tanguay, Arch. Toxicol. **85**, 787–798 (2011)
14. N.R. Mathewsa, C. Ángeles-Chávez, M.A. Cortés-Jácome, J.A. Toledo Antonio, Electrochim. Acta **99**, 76–84 (2013)
15. D.M.M. Atwa, I.M. Azzouz, Y. Badr, Appl. Phys. B **103**, 161–192 (2011)
16. E. Veena, K.V. Bangera, G.K. Shivakumar, Appl. Phys. A **123**, 366–378 (2017)
17. O.A. Castelo-González, M. Sotelo-Lerma, J.A. García-Valenzuela, J. Electron. Mater. **46**, 393–400 (2017)
18. A. Carrillo-Castillo, A. Salas-Villasenor, I. Mejia, Thin Solid Films **520**, 3107–3110 (2012)
19. A.B. Rohom, A.R. Lande, S.I. Patil, N.B. Chaure, IEEE Proc. (IEEE Xplore Digital Library) 46–48 (2013)
20. F.G. Hone, F.B. Dejene, J. Mater. Sci. Mater. Electron. **28**, 5979–5989 (2017)
21. N.B. Chaure, S. Bordas, A.P. Samantilleke, S.N. Chaure, J. Haigh, I.M. Dharmadasa, Thin Solid Films **437**, 10–17 (2003)
22. M. Piryaei, E. G. Hatam, N. Ghobadi, J. Mater. Sci. Mater. Electron. **28**, 2550–2556 (2017)

23. T.O. Berestok, D.I. Kurbatov, N.M. Opanasyuk, A.D. Pogrebnjak, O.P. Manzhos, S.M. Danilchenko, J. Nano Electron. Phys. **5**, 1009 (2013)
24. P.U. Londhe, A.B. Rohom, G.R. Bhand, S. Jadhav, M.G. Lakhe, N.B. Chaure, J. Mater. Sci. Mater. Electron. **28**, 5207–5214 (2017)
25. G. Brückmann, Kolloidzeitschrift **65**, 148–161 (1933)
26. G. Hodes, *Chemical Solution Deposition of Semiconductor Films*. (Marcel Dekker, New York, 2002)
27. B.D. Cullity, S.R. Stock, *Elements of X-ray Diffraction*. (NJ Prentice-Hall Inc, Englewood Cliff, 2001)
28. S. Nawale, V. Ravi, I.S. Mulla, Sens. Actuators B **139**, 466–470 (2009)
29. G.R. Bhand, M.G. Lakhe, A.B. Rohom, P.U. Londhe, S.K. Kulkarni, N.B. Chaure, J. Nanosci. Nanotechnol. **17**, 1–7 (2017)
30. S. Gupta, D. Patidar, N. S. Saxena, K. Sharma, Chalcogenide Lett. **6**, 723–731 (2009)